Scripta Materialia 181 (2020) 82–85

Contents lists available at ScienceDirect

Scripta Materialia

journal homepage: www.elsevier.com/locate/scriptamat

Dramatic grain refinement and magnetic softening induced by Ni addition in Fe–B based nanocrystalline soft magnetic alloys

Z. Li[a], R. Parsons[a], B. Zang[a], H. Kishimoto[b], T. Shoji[b], A. Kato[b], J. Karel[a], K. Suzuki[a,*]

[a] Department of Materials Science and Engineering, Monash University, Clayton, VIC 3800, Australia
[b] Toyota Motor Corporation, Mishuku, Susono, Shizuoka 410-1193, Japan

ARTICLE INFO

Article history:
Received 1 February 2020
Revised 9 February 2020
Accepted 9 February 2020

Keywords:
Rapid solidification
Amorphous alloys
Rapid annealing
Grain size
Coercivity

ABSTRACT

The effects of Ni addition on the grain size (D) and coercivity (H_c) were investigated for nanocrystalline $(Fe_{1-x}Ni_x)_{86}B_{14}$ (x = 0–0.3) alloys prepared by ultra-rapid annealing of melt-spun amorphous precursors. Ni addition resulted in a structural change of the nanocrystallites from bcc to fcc and an exceptionally small D of 4.2 nm was obtained at x = 0.3. H_c was reduced dramatically from 6.8 A/m at x = 0 to as small as 2.6 A/m at x = 0.1. This significant improvement of magnetic softness is well understood by the effect of Ni on the local magnetocrystalline anisotropy.

The procedure of quenching and subsequent annealing is a common approach used in engineering alloys to control the microstructure [1]. This approach has been very effective in nanocrystalline soft magnetic alloys [2,3] where fine microstructures with a grain size of about 10 nm are obtained by crystallization of melt-spun amorphous precursors. The amorphous precursors in the vast majority of alloys developed to date [4] contain non-ferromagnetic additives for accelerating the nucleation frequency and inhibiting the crystal growth process during nano-crystallization [5]. However, these additives have the unwanted effect of reducing the saturation magnetic polarization (J_s) because they are non-ferromagnetic. Recently, it has been demonstrated [6] that a soft magnetic nanostructure can be prepared even in a simple Fe–B binary system where J_s as high as 1.9 T is realized with a low coercivity (H_c) less than 8 A/m (0.1 Oe). This J_s value is comparable to that of Si steels and the coercivity corresponds to 1/4 of that of Si steels [7].

The excellent soft magnetic properties of nanocrystalline alloys are brought about by the exchange averaging of the local magnetocrystalline anisotropy energy (K_1). This averaging effect has been modelled successfully by Herzer [8,9] and his random anisotropy model predicts that H_c is proportional to the 6^{th} power of (D/L_0) where D is the grain size and L_0 is the natural exchange length. The small grain size in the Fe-B based nanocrystalline soft magnetic alloys are obtained by annealing the amorphous precursors ultra-rapidly. However, the mean grain size of these ultra-rapidly annealed (URA) alloys is around 15–20 nm [6], slightly larger than that (10 nm) of the well-established alloys such as $Fe_{74.5}Si_{13.5}B_9Nb_3Cu_1$ [2]. Hence, there is a room for improvement of the magnetic softness in the URA alloys by either refining the microstructure or enhancing L_0. Since L_0 is inversely proportional to the square root of K_1 [9], lowering K_1 is an effective approach for improving the soft magnetic properties, in addition to reducing the grain size. In this study we have investigated the effect of Ni addition because Ni is known to suppress K_1 in bcc-Fe [10]. Our aim is to clarify the effect of Ni on the grain size and the coercivity for nanocrystalline $Fe_{86}B_{14}$.

Fe-Ni-B ingots were prepared by melting mixtures of Fe (99.98%), Ni (99.9%) and B (99.9%) pieces in an Ar arc furnace. Alloy ribbons with a thickness of 15–20 μm and a width of 1 mm were prepared by a single roller melt spinner. The as-spun ribbons were cut into strips and then wrapped by a 0.02 mm thick copper foil. The packed samples were annealed in between a pair of copper blocks which were pre-heated and maintained at the annealing temperature (T_a) and pressed by a 60 N force for 0.5 s. Samples were characterized by X-ray diffraction (XRD) using a BRUKER D8 ADVANCE diffractometer with Cu $K\alpha$ radiation and a FEI TECNAI T20 transmission electron microscope (TEM) operated at 200 kV. The coercivity and saturation magnetic polarization were measured by a DC B–H tracer and a vibrating-sample magnetometer, respectively. The error of the coercivity was established by measuring 6 to 9 samples.

* Corresponding author.
E-mail address: Kiyonori.suzuki@monash.edu (K. Suzuki).

https://doi.org/10.1016/j.scriptamat.2020.02.020
1359-6462/

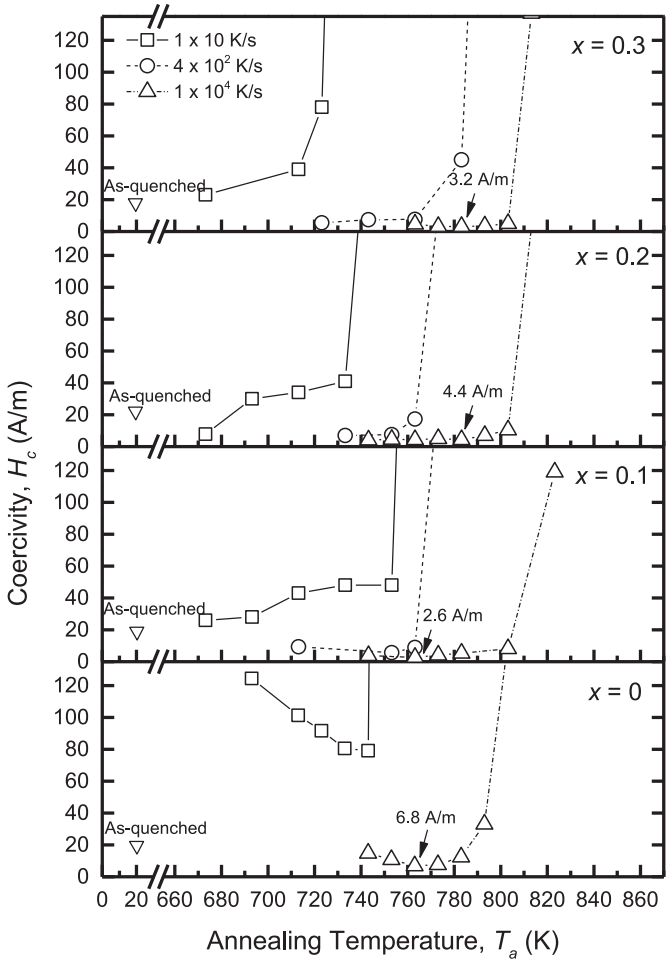

Fig. 1. Change in the coercivity as a function of annealing temperature for $(Fe_{1-x}Ni_x)_{86}B_{14}$ (x = 0, 0.1, 0.2 and 0.3) alloys.

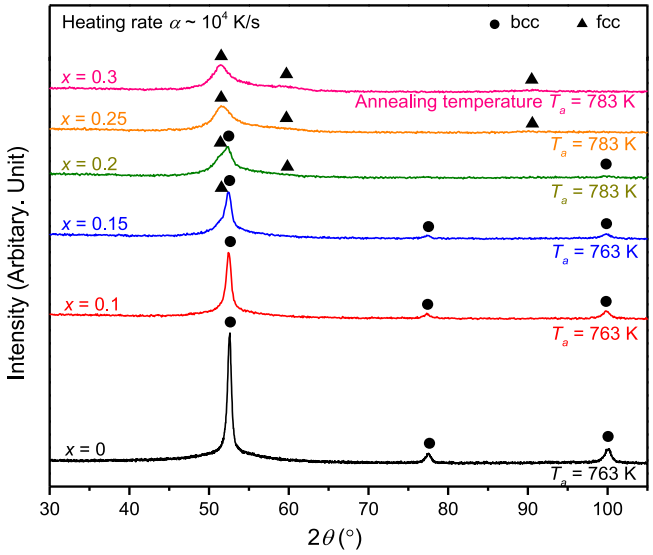

Fig. 2. X-ray diffraction patterns for nanocrystalline $(Fe_{1-x}Ni_x)_{86}B_{14}$ (x = 0, 0.1, 0.2 and 0.3) alloys ultra-rapidly annealed at the optimum temperature for the lowest coercivity.

To clarify the formation range of an amorphous phase in melt-spun $(Fe_{1-x}Ni_x)_{86}B_{14}$ (x = 0 to 0.5) alloys, the structure of the ribbons in an as-quenched state was investigated by XRD. As a result, a broad reflection characteristic of amorphous alloys was confirmed for x up to 0.3 whereas the (111) reflection from fcc-Fe(Ni) was evident for samples with $x > 0.3$, suggesting that the glass formability of $Fe_{86}B_{14}$ is affected by Ni addition. This is natural because the minimum amount of B required for full amorphization by melt-spinning in the Ni–B binary system was reported to be around 18 at% [11], considerably higher than that (13 at%) for the Fe–B binary system [6]. Since poorly quenched amorphous precursors with quenched-in crystallites often lead to deterioration of the magnetic softness in the resultant nanocrystalline state, we focus on the $(Fe_{1-x}Ni_x)_{86}B_{14}$ alloys with x up to 0.3.

In Fig. 1 we show the change in the coercivity as a function of annealing temperature for $(Fe_{1-x}Ni_x)_{86}B_{14}$ (x = 0, 0.1, 0.2 and 0.3) alloys. The ribbon samples were annealed between 673 K and 823 K with three heating rates between 10 K/s and 10^4 K/s. The onset of primary crystallization determined by differential thermal analysis with a heating rate of 0.67 K/s (results not shown) was found to be 665 ± 5 K for amorphous $(Fe_{1-x}Ni_x)_{86}B_{14}$ (x = 0, 0.1, 0.2 and 0.3) alloys. The annealing temperatures applied here were above this onset temperature. A similar experiment has already been carried out for $Fe_{87}B_{13}$, and the coercivity after primary crystallization showed a dramatic decrease with increasing heating rate [6]. The results in Fig. 1 trace the same trend and the lowest coercivity for $Fe_{86}B_{14}$ (6.8 A/m) is obtained by ultra-rapid annealing. A marked increase in H_c seen at the highest end of annealing temperature is due to the secondary crystallization reaction where a magnetically hard tetragonal-Fe_3B forms [6]. A similar trend is also seen for all the $(Fe_{1-x}Ni_x)_{86}B_{14}$ alloys with x = 0.1, 0.2 and 0.3 and the lowest coercivity is obtained consistently when the highest heating rate is applied. The minimum H_c value obtained after annealing for each alloy is marked by an arrow in the figure. The marked H_c values of the Ni containing alloys are all lower than that of the base $Fe_{86}B_{14}$ alloy, indicating that the magnetic softness of ultra-rapidly annealed Fe–B alloys is improved by Ni addition. As a result, an exceptionally low coercivity of 2.6 A/m is obtained for $(Fe_{0.9}Ni_{0.1})_{86}B_{14}$ with a saturation polarization of 1.70 T. This H_c value is one of the lowest reported to date for Cu-free nanocrystalline alloys [4].

The structure of the $(Fe_{1-x}Ni_x)_{86}B_{14}$ alloys annealed ultra-rapidly with a heating rate of 10^4 K/s at the temperature where the minimum H_c value was obtained, the optimum annealing temperature hereafter, were investigated by XRD. The results are shown in Fig. 2 where the XRD patterns for x = 0.15 and 0.25 are also included. Reflections from bcc-Fe(Ni) are confirmed on the patterns of $(Fe_{1-x}Ni_x)_{86}B_{14}$ with x up to 0.2 whereas the bcc peaks are absent from the patterns of x = 0.25 and 0.3 alloys. Instead, reflections from fcc-Fe(Ni) are evident in these two patterns. The XRD patterns of the x = 0.15 and 0.2 alloys contain reflections from both bcc- and fcc-Fe(Ni), indicating that the primary crystallization product becomes two phases. A similar effect of Ni on the structure of Fe-based nanocrystalline alloys has been reported for other alloy systems [12–14]. Since Ni is a well-known austenite stabilizer, the observed change in the crystal structure of the primary Fe precipitates is understood readily by the dissolution of Ni in Fe. Judging by the equilibrium phase diagram of Fe–Ni binary alloys [15], the α- and γ-Fe phases coexist in a wide compositional range between 5 and 28 at% Ni at the vicinity of the annealing temperatures used in the present study. This range is considerably wider than that observed for the $(Fe_{1-x}Ni_x)_{86}B_{14}$ alloys after primary crystallization. However, the composition range of the α/γ two-phase region in the Fe-Ni binary system is known to depend greatly on heating and cooling conditions [16], presumably because the full equilibrium state is hardly attained in practical processing conditions. Thus, the narrower composition range for the α/γ two-phase region in the $(Fe_{1-x}Ni_x)_{86}B_{14}$

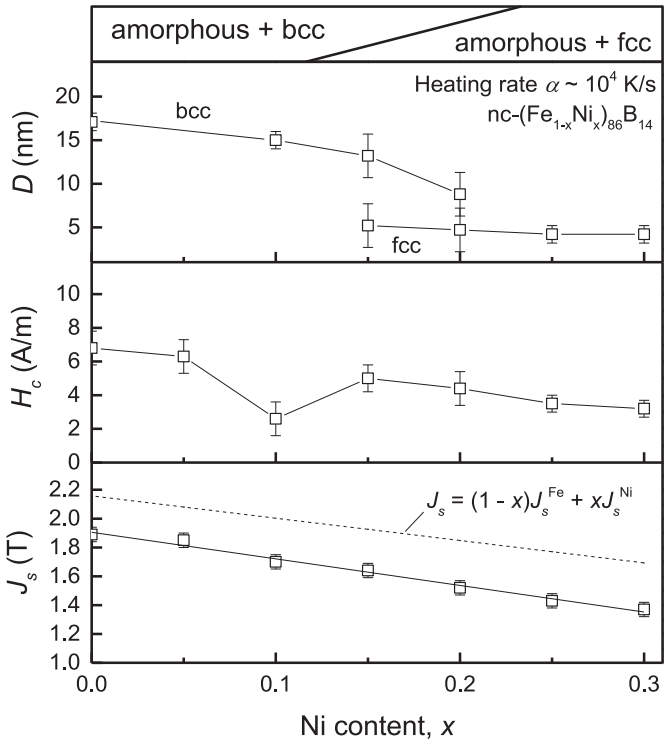

Fig. 3. Changes in the mean grain size (D), coercivity (H_c) and saturation magnetic polarization (J_s) for nanocrystalline $(Fe_{1-x}Ni_x)_{86}B_{14}$ alloys as a function of Ni content (x).

alloys is attributable to the high heating rate employed for annealing.

In Fig. 3 we show the changes in the mean grain size (D), the coercivity (H_c) and the saturation magnetic polarization (J_s) as a function of Ni content for the $(Fe_{1-x}Ni_x)_{86}B_{14}$ alloys after optimum annealing. The grain size was estimated from the peak broadening effect on the XRD reflections. The grain size remains between 15 and 17 nm for x up to 0.1 where the nanocrystallites are bcc-Fe. However, a dramatic decrease in D to 4.2 nm is seen above $x = 0.2$ where the nanocrystallites become predominantly fcc-Fe. This extremely fine microstructure was also confirmed by direct microstructural observations. Fig. 4 shows the bright- and dark-field TEM images along with the selected area diffraction (SAD) patterns for nanocrystalline $(Fe_{1-x}Ni_x)_{86}B_{14}$ ($x = 0$ and 0.3) alloys after optimum annealing. The SAD patterns confirm that the crystallites in the $x = 0$ and 0.3 alloys are bcc-Fe and fcc-Fe, respectively. The dark-field images were constructed by placing the objective aperture on the $\{110\}_{bcc}$ ring of the $x = 0$ alloy and the $\{111\}_{fcc}$ ring of the $x = 0.3$ alloy. For the Ni-free $Fe_{86}B_{14}$ alloy, bcc-Fe grains with sizes of 10 to 20 nm are seen while the grain size of fcc-Fe in the $(Fe_{0.7}Ni_{0.3})_{86}B_{14}$ alloy is well below 10 nm. The volume-weighted average of the grain size estimated from the TEM images of $(Fe_{0.7}Ni_{0.3})_{86}B_{14}$ by the autocorrelation function [17] is 4 ± 1 nm, fully consistent with the result (4.2 nm) estimated from the XRD pattern. Given the fact that the mean grain size of the well-known nanocrystalline Fe–Si–B–Nb–Cu alloys is typically around 10 nm, the grain size of nanocrystalline $(Fe_{0.7}Ni_{0.3})_{86}B_{14}$ appears to be exceptionally small. This is striking because the precursor amorphous ribbon contains none of the commonly used additives such as Nb and Cu for grain refinement. The grain refinement effect induced by Nb in nanocrystalline $Fe_{73.5}Si_{13.5}B_9Nb_3Cu_1$ is believed to be due to the large partitioning behaviour of Nb between the primary crystalline and the residual amorphous phases. However, this mechanism is irrelevant to the refinement induced by Ni simply because Ni is soluble in the primary crystalline phase and Nb-type partitioning behaviour is unlikely. Hence, the exceptionally fine microstructure of nanocrystalline $(Fe_{0.7}Ni_{0.3})_{86}B_{14}$ should be attributed to accelerated nucleation kinetics of the fcc-Fe(Ni) phase. A crude but possible argument for explaining the high nucleation rate of fcc-Fe(Ni) is the interfacial energy between the nuclei and the amorphous matrix. It is well known that the coordination number of Fe atoms in Fe-based amorphous alloys is around 12 [18]. Thus, the interfacial misfit is expected to be smaller for nuclei with closed-packed structures. This may explain the difference in the grain size between the bcc-Fe(Ni) and fcc-Fe(Ni) nanocrystallites formed on primary crystallization of amorphous $(Fe_{1-x}Ni_x)_{86}B_{14}$ alloys.

The coercivity of the nanocrystalline $(Fe_{1-x}Ni_x)_{86}B_{14}$ alloys in Fig. 3 shows a clear decrease from 6.8 A/m at $x = 0$ to 2.6 A/m at $x = 0.1$. This can be explained by the dissolution of Ni in bcc-Fe. We have confirmed that the coercivity of our ultra-rapidly annealed nanocrystalline alloys (HiB-Nanoperm) can be described by the random anisotropy model [8,9]. It was found that the well-known D^6 dependence was seen for $H_c > 20$ A/m while the dependence becomes D^3 below this coercivity [19]. The later D^3 dependence has been seen for samples with a strong influence of induced anisotropies (K_u) [20] where the exchange-averaged magnetic anisotropy ($<K>$) is given by [9]

$$K \approx K_u + \frac{1}{2} v_{cr} \sqrt{\beta K_1 K_u} \left(\frac{D}{L_0}\right)^3 \quad (1)$$

Here, v_{cr} is the volume fraction of the crystalline phase, the parameter β is about 0.4 for bcc-Fe and the natural exchange length (L_0) is determined by

$$L_0 = \varphi \sqrt{\frac{A}{K_1}}, \quad (2)$$

where A is the exchange stiffness constant and φ is a dimensionless parameter around unity. When K_u is coherent, the random magnetocrystalline anisotropy ($<K_1>$) relevant to the coercivity is determined by the 2nd term in Eq. (1) which is proportional to $K_1{}^2$. Judging by the compositional dependence of the intrinsic magnetocrystalline anisotropy in Fe–Ni binary alloys [10], K_1 is reduced from 52 kJ/m^3 to 31 kJ/m^3 by an addition of 10 at% Ni to pure Fe. Adopting this extent of K_1 reduction, $\langle K_1 \rangle$ in $(Fe_{0.9}Ni_{0.1})_{86}B_{14}$ is expected to be about a third of that in the Ni-free alloy, accounting for the observed difference in H_c between the two alloys well.

The H_c in Fig. 3 shows an increase from 2.6 A/m to 5.0 A/m between $x = 0$ and 0.15. This composition range corresponds to the phase boundary where the fcc-Fe(Ni) starts to form after nanocrystallization. Fe-rich Fe–Ni alloys have attracted much attention owing to the Inver behaviour [21,22] where an anomaly of the Curie point (T_C) is seen. The Curie point of fcc-Fe–Ni alloys is reduced dramatically by increasing Fe content, and it approaches room temperature at the most Fe-rich phase boundary [16,21]. Hence, the fcc-Fe(Ni) nanocrystallites formed at the most Fe-rich boundary ($x = 0.15$) are expected to have a low T_C possibly below room temperature. Since T_C is a reflection of the exchange integral, the fcc-Fe(Ni) nanocrystallites in $(Fe_{0.85}Ni_{0.15})_{86}B_{14}$ are expected to become the weakest link in the exchange coupled spin chain, which limits the exchange length and thus, the averaging effect [23]. This explains the minimum H_c value at $x = 0.1$. However, this weak coupling effect should be suppressed in alloys richer in Ni because T_C in fcc-Fe(Ni) is known to increase with increasing Ni content. Hence, the coercivity of the nanocrystalline $(Fe_{1-x}Ni_x)_{86}B_{14}$ alloys shows a gradual decrease between $x = 0.15$ and 0.3.

The saturation polarization (J_s) of nanocrystalline $(Fe_{1-x}Ni_x)_{86}B_{14}$ shows a monotonous decrease from 1.89 T at $x = 0$ to 1.37 T at $x = 0.3$ with an average gradient of – 1.84 T/x.

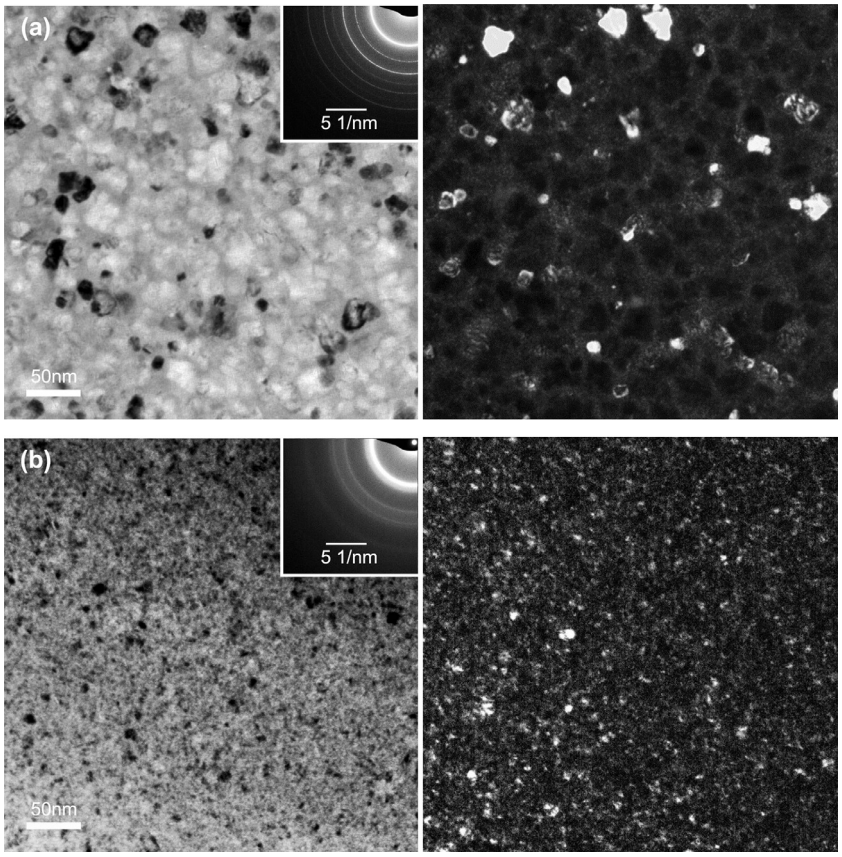

Fig. 4. Bright- and dark-field transmission electron micrographs and selected area electron diffraction patterns for (a) $Fe_{86}B_{14}$ annealed at 763 K for 0.5 s and (b) $(Fe_{0.7}Ni_{0.3})_{86}B_{14}$ annealed at 783 K for 0.5 s. The heating rate for annealing was 10^4 K/s.

This rate of decrease in J_s is slightly steeper than that (–1.55 T/x) for the simple weighted average of the J_s values for pure Fe and Ni, presumably because of the Inver effect. Still, a high J_s of 1.7 T and a small H_c of 2.6 A/m are obtained for nanocrystalline $(Fe_{0.9}Ni_{0.1})_{86}B_{14}$.

The structural and magnetic properties of amorphous $(Fe_{1-x}Ni_x)_{86}B_{14}$ (x = 0 to 0.3) after ultra-rapid annealing were investigated in order to clarify the effect of Ni on the soft magnetic properties of the resultant nanocrystalline alloys. The three noteworthy outcomes from this report are as follows:

(1) The coercivity of nanocrystalline $Fe_{86}B_{14}$ is reduced dramatically from 6.8 A/m to 2.6 A/m by replacing 10 % of Fe with Ni, indicating that Ni is very effective in improving the soft magnetic properties of the Fe–B based alloys.
(2) The structure of nanocrystallites after primary crystallization is found to change from bcc to fcc at x between 0.1 and 0.25, showing that the fcc structure is stabilized by the dissolution of Ni in Fe.
(3) An exceptionally small grain size of 4.2 nm is obtained for nanocrystalline $(Fe_{0.7}Ni_{0.3})_{86}B_{14}$ where the nanocrystallites are fcc-Fe(Ni).

Acknowledgments

The authors are grateful to the Australian Research Council for its financial support. We would also like to acknowledge Monash Centre of Electron Microscopy and Monash X-Ray Platform for providing facilities and help from the staff.

References

[1] J.W. Christian, The Theory of Transformations in Metals and Alloys, Oxford, Pergamon, 2002.
[2] Y. Yoshizawa, S. Oguma, K. Yamauchi, J. Appl. Phys. 64 (1988) 6044–6046.
[3] K. Suzuki, A. Makino, A. Inoue, T. Masumoto, J. Appl. Phys. 70 (1991) 6232–6237.
[4] M.A. Willard, M. Daniil, in: Handbook of Magnetic Materials, 21, Elsevier, Amsterdam, 2013, pp. 173–342.
[5] K. Hono, Prog. Mater. Sci 47 (2002) 621–729.
[6] B. Zang, R. Parsons, K. Onodera, H. Kishimoto, A. Kato, A.C.Y. Liu, K. Suzuki, Scr. Mater. 132 (2017) 68–72.
[7] JFE Steel Cat. No. F1E-002-02: Electrical Steel Stheets for High-frequency Application, JEF Steel, Tokyo, 2014.
[8] G. Herzer, IEEE Trans. Magn. 25 (1989) 3327–3329.
[9] G. Herzer, in: H. Kronmüller, S. Parkin (Eds.), Handbook of Magnetism and Advanced Magnetic Materials, 4, John Wiley, Hoboken, 2007, pp. 1882–1908.
[10] L.P. Tarasov, Phys. Rev. 56 (1939) 1245–1246.
[11] M. Takahashi, C.O. Kim, M. Koshimura, T. Suzuki, Jpn. J. Appl. Phys. 17 (1978) 741–742.
[12] J. Turčanová, J. Marcin, J. Kováč, D. Janičkovič, P. Švec, I. Škorvánek, J. Phys. Conf. Ser. 144 (2009) 012065.
[13] N. Aronhime, E. Zoghlin, V. Keylin, X. Jin, P. Ohodnicki, M.E. McHenry, Scr. Mater. 142 (2018) 133–137.
[14] N. Aronhime, P. Ohodnicki, M.E. McHenry, Scr. Mater. 169 (2019) 9–13.
[15] L.J. Swartzendruber, V.P. Itkin, C.B. Alcock, in: P. Villars, H. Okamoto, K. Cenzual (Eds.), ASM alloy phase diagrams database, ASM International, 2016 No. 979957.
[16] R.M. Bozorth, Ferromagnetism, IEEE Press, Piscataway, 1978.
[17] B. Zang, K. Suzuki, A.C.Y. Liu, Mater. Charact. 142 (2018) 577–583.
[18] Y. Waseda, H.S. Chen, Phys. Stat. Sol. 49 (1978) 387–392.
[19] K. Suzuki, R. Parsons, B. Zang, K. Onodera, H. Kishimoto, T. Shoji, A. Kato, AIP Adv. 9 (2019) 035311.
[20] K. Suzuki, N. Ito, J.S. Garitaonandia, J.D. Cashion, G. Herzer, J. Non-Cryst. Solids 354 (2008) 5089–5092.
[21] H. Asano, J. Phys. Soc. Jpn. 27 (1969) 542–553.
[22] G. Hausch, H. Warlimon, Acta metall. 21 (1973) 401–414.
[23] K. Suzuki, J.M. Cadogan, Phys. Rev. B 58 (1998) 2730–2739.